



**HAL**  
open science

## Stable Mn-magnetite derived from Mn-siderite by heating in air

A. Isambert, J. -P. Valet, A. Gloter, F. Guyot

► **To cite this version:**

A. Isambert, J. -P. Valet, A. Gloter, F. Guyot. Stable Mn-magnetite derived from Mn-siderite by heating in air. *Journal of Geophysical Research: Solid Earth*, 2003, 108, pp. 767-782. 10.1029/2002JB002099 . insu-03598418

**HAL Id: insu-03598418**

**<https://insu.hal.science/insu-03598418>**

Submitted on 6 Mar 2022

**HAL** is a multi-disciplinary open access archive for the deposit and dissemination of scientific research documents, whether they are published or not. The documents may come from teaching and research institutions in France or abroad, or from public or private research centers.

L'archive ouverte pluridisciplinaire **HAL**, est destinée au dépôt et à la diffusion de documents scientifiques de niveau recherche, publiés ou non, émanant des établissements d'enseignement et de recherche français ou étrangers, des laboratoires publics ou privés.

Copyright

## Stable Mn-magnetite derived from Mn-siderite by heating in air

A. Isambert and J.-P. Valet

Laboratoire de Paléomagnétisme, Institut de Physique du Globe de Paris, Paris, France

A. Gloter

Laboratoire de Physique des Solides, Université Paris Sud, Orsay, France

F. Guyot

Laboratoire de Minéralogie et de Cristallographie de Paris, Institut de Physique du Globe de Paris, Paris, France

Received 17 July 2002; revised 17 January 2003; accepted 11 February 2003; published 3 June 2003.

[1] Magnetic experiments, microscopic analyses and X-ray diffractometry were conducted on oxidation products of Mn-bearing natural crystalline siderite after successive heating steps in air. Magnetic measurements indicated the production of single-domain and pseudo single domain ferrimagnetic phases with Curie temperatures between 420°C and 560°C. Hematite formation was detected by X-ray diffraction after heating the siderite samples at 480°C, while Mn-ferrite was formed at 500°C and persisted even after heating to 700°C. This final product is stable with a spinel structure and unit cell parameters intermediate between those of magnetite and maghemite. Transmission electron microscopy and electron energy loss spectroscopy analyses confirmed the presence of Mn in the spinel ferrite phase, which contains Fe(III), Mn(III), and Mn(II) ions. This phase appears as single crystals with euhedral shapes of average grain size 90–100 nm. In comparison to pure magnetite, the addition of Mn in the crystal lattice lowers the Curie temperature and explains the stability of the spinel phase. Thus stable magnetization carried by a magnetite related phase can be generated by oxidation of Mn-siderite. **INDEX TERMS:** 1519 Geomagnetism and Paleomagnetism: Magnetic mineralogy and petrology; 1540 Geomagnetism and Paleomagnetism: Rock and mineral magnetism; 1599 Geomagnetism and Paleomagnetism: General or miscellaneous; **KEYWORDS:** Mn-ferrite, Mn-magnetite, oxidation of siderite, stable magnetization

**Citation:** Isambert, A., J.-P. Valet, A. Gloter, and F. Guyot, Stable Mn-magnetite derived from Mn-siderite by heating in air, *J. Geophys. Res.*, 108(B6), 2283, doi:10.1029/2002JB002099, 2003.

### 1. Introduction

[2] Oxidation of siderite [Seguin, 1966] stands as a possible mechanism for production of magnetic phases with profound implications for paleomagnetic studies of carbonated rocks [Ellwood *et al.*, 1986; Pan *et al.*, 2000]. This mechanism has also been suggested as a possible scenario for formation of single domain crystals of magnetite in the ALH84001 SNC meteorite [MacKay *et al.*, 1996; Friedmann *et al.*, 2001; Thomas-Keptra *et al.*, 2000, 2001].

[3] Siderite (FeCO<sub>3</sub>) is an iron bearing carbonate, common in marine and lacustrine environments. This is an antiferromagnetic mineral with a Néel temperature of 38 K, which is paramagnetic at ordinary temperature. Thermal decomposition and oxidation of the mineral siderite has previously been studied, with two major interests. Siderite has been shown to decompose in air into magnetite and maghemite and then into hematite [Ellwood *et al.*, 1986; Pan *et al.*, 2000] and thus can potentially carry a chemical remanent magnetization with consequences for paleomagnetic studies. The second interest is that magnetite present in

the ALH84001 Martian meteorite is associated with carbonate globules (MgCO<sub>3</sub>-FeCO<sub>3</sub> solid solution with variable Ca and Mn content). Thomas-Keptra *et al.* [2000] defended that the morphologies and grain sizes of magnetites were typical of biogenic origin. However, a second possibility is that magnetite of ferrous carbonates in ALH84001 would result from oxidation of siderite [Brearley, 1998; Barber and Scott, 2002; Golden *et al.*, 2001; Koziol, 2001].

[4] The samples were collected from the Saint Georges d'Hurtière iron mine, Savoie, France, and contain approximately 13 and 6% substitution of Fe by Mn and Mg, respectively. Conventional magnetic methods were used as a mineralogical tool in order to identify the mineralogical transformations and to characterize the new magnetic phases formed during decomposition of siderite with temperature. Observations by transmission electron microscopy, X-ray diffraction (XRD), and electron energy loss spectroscopy were performed in parallel.

### 2. Experimental Methods

[5] Cylindrical samples (2.3 cm in diameter and 11 cm<sup>3</sup> in volume), drilled from the block samples were used for

measurements of magnetization. Powders were used for XRD, transmission electron microscopy (TEM), and magnetic susceptibility measurements of temperature-annealed samples.

[6] The magnetic susceptibility ( $\kappa$ ) cycles were measured on a CS2-KLY2 susceptibilimeter with a relative precision of  $10^{-8}$  and a temperature accuracy of  $5^\circ\text{C}$ . The remanence measurements were conducted on a JR5 spinner magnetometer (noise level:  $5 \times 10^{-9} \text{ A m}^2$ ) after thermal treatment of massive cylindrical siderite. Isothermal remanent magnetization (IRM) and hysteresis cycles were performed with a high field inductometer with a  $5 \times 10^{-7} \text{ A m}^2$  sensitivity. Precision of magnetic measurements is about 3 to 5% and accuracy of the field measurements is 0.5 mT.

[7] The powder samples used for magnetic measurements were then directly analyzed by TEM and XRD. TEM analyses were conducted on a TOPCON Ø02B TEM equipped with a LaB<sub>6</sub> gun and a modified Gatan PEELS 666 electron energy loss spectrometer. The transmission electron microscope has a point-point resolution of 0.19 nm, which is sufficient to provide high-resolution electron microscopy (HREM) images of the major lattice fringes in siderite, magnetite, and hematite crystals. The electron energy loss spectra (EELS) were collected in diffraction mode at 100 kV using homemade lenses coupled with a CCD detection system. The original resolution in energy of the system is around 0.8 eV for core loss spectra (O 1s, Mn 2p, Fe 2p). Energy resolution of the EELS spectra were subsequently improved to 0.3–0.4 eV using Richardson-Lucy numerical restoration [Gloter *et al.*, 2003]. X-ray diffraction analyses were carried out on a Philips PW1710 diffractometer using CoK $\alpha$  radiation (40 kV; 30 mA; start angle ( $^\circ 2\theta$ ): 15.000; end angle ( $^\circ 2\theta$ ): 80.000; step size ( $^\circ 2\theta$ ): 0.040; time per step (seconds): 30.000). Thermal gravity analyses (TGA) were obtained at the CRISMAT ISMRA laboratory of Caen University on a SETARAM TGA 92 type apparatus equipped with a B92 electronic microscale and a graphite resistor oven. The limit of detection of mass changes is 1 microgram.

### 3. Characterization of the Initial Material

[8] Optical microscopy observations revealed that the samples essentially consist of well-crystallized millimeter-sized grains of siderite. Quartz, iwakiite (MnFe<sub>2</sub>O<sub>4</sub>), and hematite were also occasionally detected. The siderite is Mn and Mg rich. The EPMA analyses conducted on a CAMECA SX50 (nine analyses, Table 1) indicate the following formula: Fe<sub>0.79(2)</sub>Mn<sub>0.12(2)</sub>Mg<sub>0.07(2)</sub>Ca<sub>0.02(1)</sub>CO<sub>3</sub>. The unit cell parameters ( $a = 4.702 \text{ \AA}$ ,  $c = 15.401 \text{ \AA}$ ) are given in Table 2. The slight increase in  $a$  and  $c$  with respect to pure siderite is

**Table 1.** Electron Probe Microanalysis of Siderite Starting Material

Element	Analysis <sup>a</sup>								
	1	2	3	4	5	6	7	8	9
Ca	0.70	0.62	0.64	0.82	1.03	0.93	0.91	0.76	0.93
Mn	5.46	6.19	6.16	6.49	5.88	6.07	6.63	5.73	6.14
Fe	40.52	39.16	38.82	39.02	40.03	39.73	39.35	39.98	38.87
Mg	3.32	4.03	4.38	3.67	3.07	3.26	3.11	3.53	4.06
O	50.00	50.00	50.00	50.00	50.00	50.00	50.00	50.00	50.00

<sup>a</sup>Atom % normalized to siderite structural formula.

**Table 2.** Refinement From Powder Diffraction Data

Phase	Temperature, <sup>a</sup> °C	Crystal System	Parameter	Value	Sample - Standard <sup>b</sup>
Siderite	unheated	hexagonal	a	4.702	0.009
			c	15.401	0.021
Siderite	480	hexagonal	a	4.697	0.004
			c	15.395	0.015
Siderite	530	hexagonal	a	4.697	0.004
			c	15.398	0.018
Hematite	480	hexagonal	a	5.019	-0.034
			c	13.735	-0.004
Hematite	530	hexagonal	a	5.033	-0.020
			c	13.704	-0.036
Mn-ferrite	530	cubic	a	8.352	-0.043
Mn-ferrite	700	cubic	a	8.370	-0.026

<sup>a</sup>Standard used for Mn-ferrite:magnetite.

<sup>b</sup>Annealing temperature. All spectra recorded at ambient conditions.

consistent with prominent Mn-Fe substitution since MnCO<sub>3</sub> has larger unit cell parameters ( $a = 4.790 \text{ \AA}$ ,  $c = 15.69 \text{ \AA}$ ) than FeCO<sub>3</sub> ( $a = 4.693 \text{ \AA}$ ,  $c = 15.38 \text{ \AA}$ ). TEM analyses of the initial material confirm the presence of siderite with a minor amount of hematite. Hematite appears as well-crystallized rod-shaped grains, a few micrometers in size. EELS spectra at Fe  $L_{2,3}$  and Mn  $L_{2,3}$  edges of siderite and hematite are shown in Figure 1. For comparison, we show the spectra obtained with the same experimental conditions for reference samples of hematite (Ouro Preto mines, Brazil) and magnetite (Aldrich chem., synthetic). The iron  $L_{2,3}$  edges of siderite compare well with the one obtained by Garvie *et al.* [1994] using a cold field STEM-VG operating at 0.45 eV energy resolution. Our spectrum exhibits more clearly the two weak shoulders (marked by arrows) on both sides of the  $L_3$  line. Note that they were restored from part of the energy spread of the incident beam, of the spectrometer aberrations, and of CCD point spread function using inverse problem algorithm [Gloter *et al.*, 2003]. As these features have already been observed for Fe<sup>2+</sup> ions using X-ray absorption spectroscopy (XAS) [Peng *et al.*, 1995], we believe that this observation results from slight improvements in resolution with respect to Garvie *et al.* [1994]. The Fe  $L_{2,3}$  spectrum of hematite from the initial material compares well with the reference sample. In addition, they are both in good agreement with the characteristics described in literature for EELS or XAS at Fe 2p edge for pure Fe<sup>3+</sup> compounds [Van Aken *et al.*, 1998; Garvie and Buseck, 1998]. The spectra recorded at the Mn  $L_{2,3}$  edges in siderite compare well with pure Mn<sup>2+</sup> bearing rhodocrosite published by Garvie *et al.* [1994]. The Mn spectrum collected for the hematite phase shows two broad white lines and a much higher  $L_3/L_2$  ratio. In addition, the maximum of the  $L_3$  line is shifted by about 1.5 eV toward higher energy with respect to the  $L_3$  line of siderite. This is a strong indication for a higher Mn valency state in hematite than in siderite. The absence of clearly legible fine structure in the  $L_3$  line indicates a preponderance of the trivalent state for Mn ions. Indeed, Mn<sup>4+</sup> would exhibit a sharp peak at the lower side of a broad  $L_3$  line [Cressey *et al.*, 1993].

## 4. Results

### 4.1. Thermal Gravity Analysis (TGA)

[9] In Figure 2 we plotted the mass changes in the samples between ambient temperature and 700°C (heating rate of 5°C/hr). The moderate and continuous mass loss

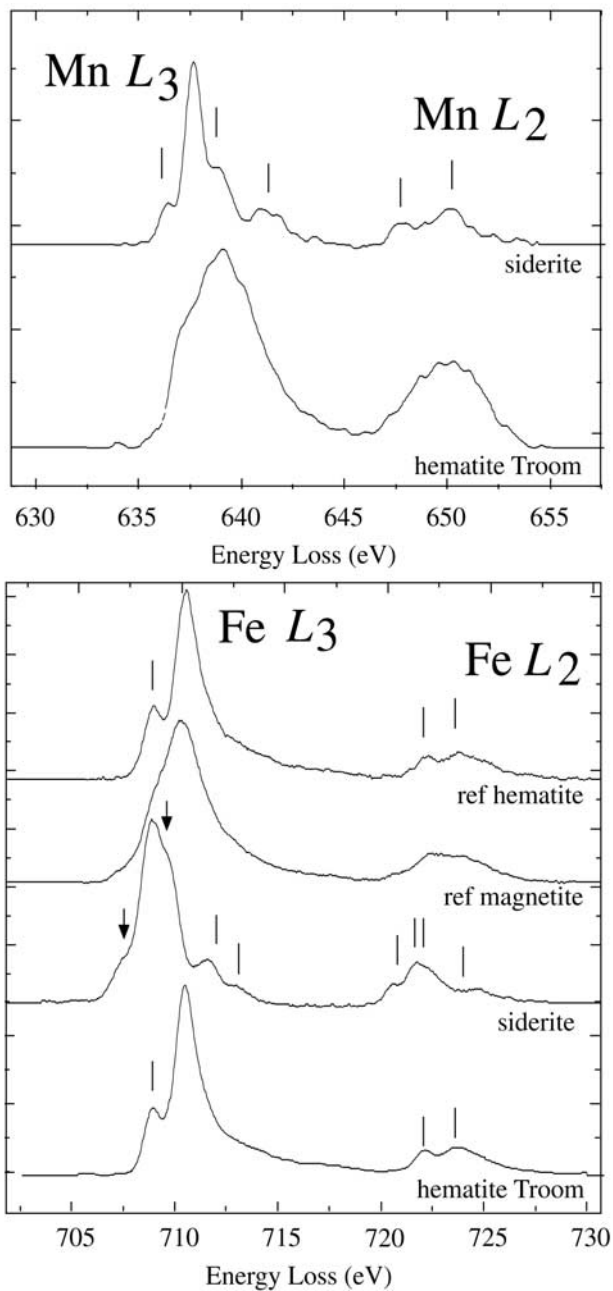


**Figure 1.** EELS spectra at Mn  $L_{2,3}$  and Fe  $L_{2,3}$  edges of the initial material.

between 25°C and 400°C (about 4%) is ascribed to combination of dehydration or residual water and to slight oxidation of siderite (see below). Between 450°C and 550°C, the mass decreases abruptly due to decarbonation, and stabilizes at 73% of the total initial mass at 550°C.

## 4.2. Thermomagnetic Experiments

### 4.2.1. First Susceptibility Cycle

[10] The samples were heated up to 700°C and cooled down to room temperature (Figure 3). Between 25°C and 270°C, the low-field susceptibility ( $\kappa$ ) remained very weak due to the antiferromagnetic behavior of the mineral. Susceptibility increased regularly beyond 270°C indicating production of a new magnetic phase. A maximum at about

430°C was followed by a decrease down to 480°C, which is likely due to a new magnetic phase with larger susceptibility but relatively low Curie temperature. A second bump appeared between 500°C and 520°C, which indicates that a second mineral has been produced with a Curie temperature close to that of pure magnetite. Cooling is characterized by a very sharp and abrupt increase by up to 6 orders of magnitude below 510°C, which reaches the values measured during the heating experiment. There is a maximum at 470°C, typical of a Hopkinson-type effect. Then  $\kappa$  decreases slowly but weakly with respect to the previous change. These experiments indicate the unstable character of siderite upon heating. The high-temperature curve depicts two successive mineralogical transformations between 300°–430°C and at 500°C, respectively.

### 4.2.2. Subsequent Cycles

[11] A total of three successive susceptibility cycles were carried out in order to characterize further the transformations of siderite with temperature and time (Figure 4). Indeed, it was likely that the initial sample was not totally transformed during the first 90 min cycle up to 520°C. The second cycle was performed up to 700°C and confirmed that transformations were still occurring. As expected the previous cooling and the new heating curves match well with each other, but there was again a significant increase of  $\kappa$  during the second cooling. The same scenario was repeated during the third cycle. The most noticeable observation was that the new phase formed after each heating exhibited a different Curie temperature than during the previous cycle. Each cycle showed a noticeable Hopkinson peak, but it was observed at higher temperature during the second cooling than during the third cooling. This could be caused by changes in composition of the newly formed magnetic phase. However, Curie temperature of superparamagnetic grains, which generate the Hopkinson peak, can be very sensitive to small variations in size.

[12] In summary, new magnetic phases formed upon heating of siderite. In each case, there was irreversibility between the heating and the cooling curves but reversibility between the cooling and the subsequent heating curve.

### 4.2.3. Hysteresis Cycles

[13] Hysteresis cycles were performed with a high field inductometer on siderite powder at room temperature and

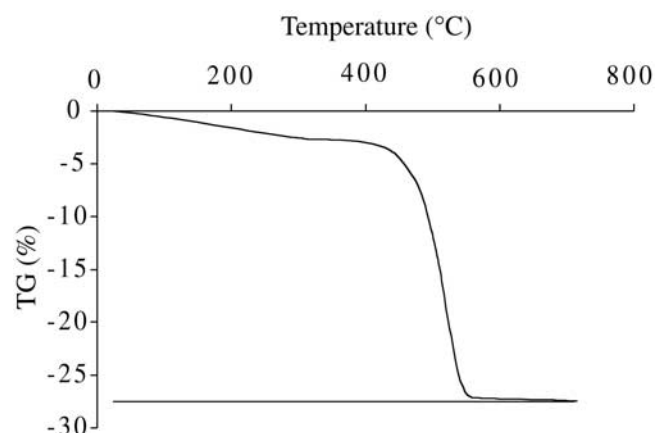


**Figure 2.** Thermal gravity analysis for samples heated from ambient temperature up to 700°C.

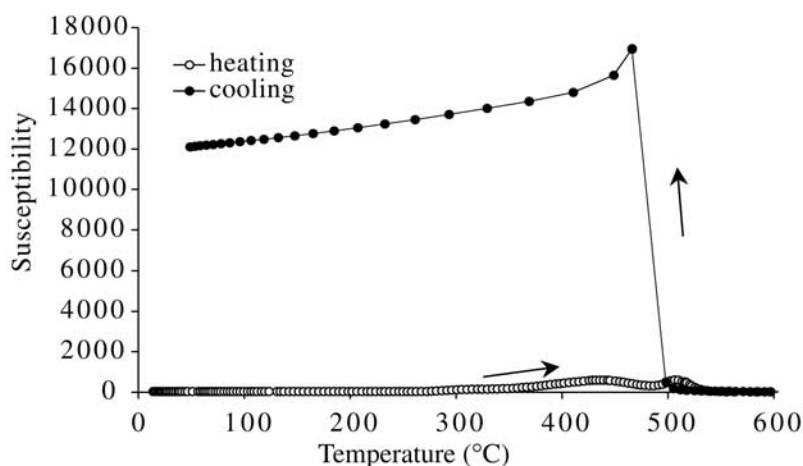


**Figure 3.** Simple susceptibility cycle up to 700°C.

after heating at 480°C, 530°C, and 700°C (Figure 5). The induced magnetization of unheated siderite increased regularly with the applied field and showed no saturation after 1 Tesla as expected for a dominant paramagnetic mineral. This is consistent with the presence of siderite and hematite, both antiferromagnetic minerals with paramagnetic behavior above the Néel temperature ( $T_N = 38$  K for siderite). The results obtained after each heating cycle were quite consistent with the thermomagnetic analyses as they revealed an increased proportion of ferromagnetism with increasing temperatures. The coercivity of remanence (16.14, 19.75, and 21.09 mT for 480°C, 530°C, and 700°C, respectively) is rather low. Saturation ( $M_s$ ) was reached at 0.2 T ( $H_{sat}$ ) with a coercivity of 6.45, 9.25, and 10.25 mT after heating at 480°C, 530°C, and 700°C, respectively. Saturation of remanence was measured also in heated powdered samples of siderite that were subjected to a magnetic field varying from 0 to 1 T. The measurements were performed at room temperature in zero field. Saturation remanent magnetization ( $J_{rs}$ ) of the three heated samples was reached at about 0.2 T. These results are consistent with the presence of

single domain or pseudo-single domain grains of a magnetite-related phase.

#### 4.2.4. Remanent Magnetization

[14] The initial natural remanent magnetization (NRM) of siderite was measured and then stepwise demagnetized in a zero field up to 700°C (Figure 6). As expected, siderite was characterized by null or quasi-null remanence below 460°C. However, we observed a large increase (by 1 order of magnitude) beyond 510°C. This variation is surprising since heating was performed in a zero field. The samples were protected as much as possible in  $\mu$ -metal containers during transportation and the measurements were performed in a  $\mu$ -metal shielded room. The only field present during the experiment could be the residual field of the magnetometer. Two successive measurements of the magnetization were done at 1-min interval to evaluate the stability of the remanent signal. In all cases the second value was found to be higher than the first one. The second striking feature is the absence of Curie point even after heating up to 700°C. Given the absence of remanent magnetization of the initial siderite, this result suggests that the remanent magnetization

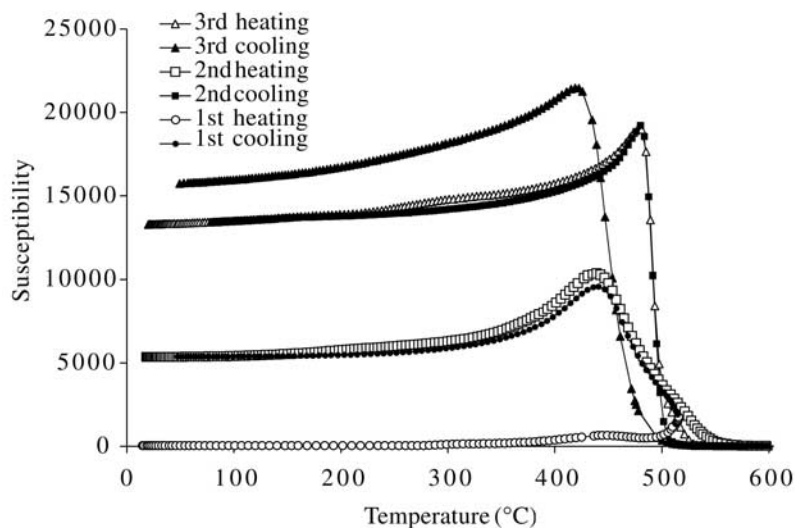


**Figure 4.** Three successive susceptibility cycles of the same specimen. Note the reversibility of the cooling and the subsequent heating curves but the irreversible character of each individual cycle.

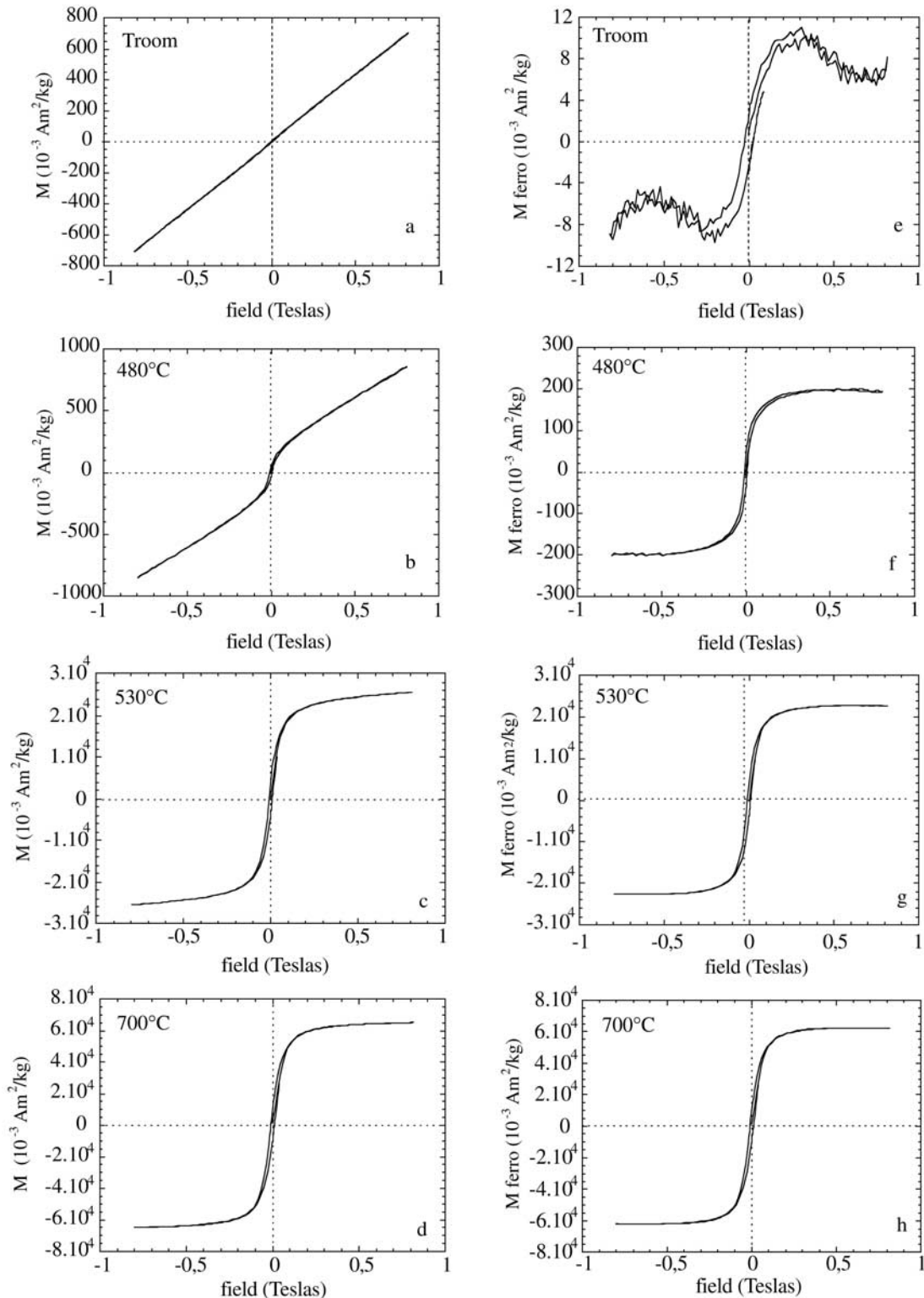


**Figure 5.** Hysteresis cycles of siderite powders at room temperature and after heating at 480°C, 530°C, and 700°C. (a–d) Noncorrected of paramagnetic effect and (e–h) corrected of paramagnetic effect.

measured above 510°C after heating in a zero field was caused by superparamagnetic grains that spontaneously oriented themselves in the small residual field of the laboratory.

#### 4.2.5. Thermoremanent Magnetization (TRM)

[15] The samples were heated in a 40 microteslas field (Figure 7). Below 300°C the TRM values did not exceed  $10^{-3} \text{ A/m}$ , but they increased significantly between 430°C

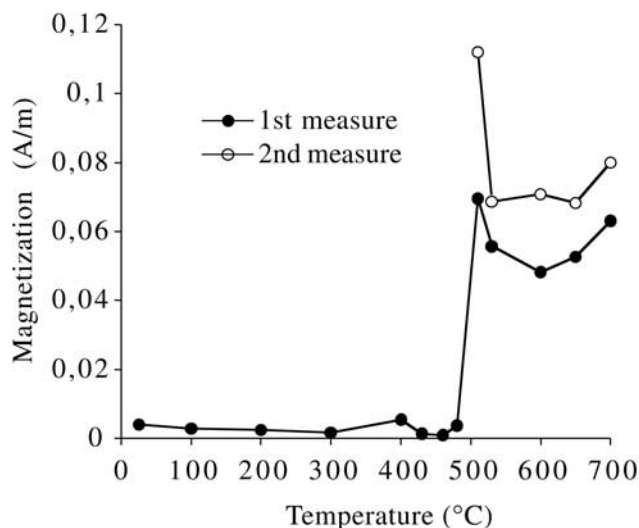


**Figure 6.** Variations of NRM during stepwise thermal demagnetization.

and 500°C. Note that the TRM acquired at this stage was 1000 times larger (100 A/m) than the remanent magnetization that was measured during the previous experiment after heating in zero field. In this case the magnetization remained stable after successive measurements and was obviously caused by highly magnetic minerals that carry a stable remanent magnetization. Beyond 600°C the TRM slightly decreased. Some loss of material subsequent to thermal cracks in the sample yielding some material desegregation and fall after repeated heatings is probably responsible for this decrease.

### 4.3. X-ray Diffractometry (XRD)

[16] X-ray diffraction was performed at ambient temperature on siderite powders loaded on hollowed aluminium plates after heating in air for 1 hour at three temperatures (480°C–530°C–700°C). X-ray diffraction spectra are shown in Figure 8, and the unit cell parameters are given in Table 2. In some samples, small amounts of hematite, iwakiite, and/or quartz are identified at room temperature (the threshold of detection is about 3%). In samples heated at 480°C the contribution of hematite increases, with relatively broad peaks. In samples heated at 530°C, hematite is still produced, but the major point is the appearance of a spinel-structured phase, which was identified as Mn-ferrite (see TEM results below). The unit cell parameters of hematite are slightly smaller than in pure hematite. In samples heated at 700°C the spectra consist exclusively of Mn-ferrite, with no detectable peaks of siderite or hematite. We thus conclude that the final oxidation product of Mn-bearing siderite heated in air is a spinel-structured phase close to magnetite and maghemite.

### 4.4. Transmission Electron Microscopy

[17] Successive TEM analyses were carried out on siderite powders after heating at 480°C, 530°C, and 700°C. In agreement with the XRD results, hematite (Figure 9), identified by electron diffraction patterns and EELS spectra (Figure 10), is shown to grow on siderite crystals upon heating at 480°C. The newly formed hematite phase con-

sists of small crystals with an average size of 20 nm, in some cases smaller than 5 nm, in any case much smaller than those of hematite present in the initial material. The EELS spectra of the newly formed hematite revealed the presence of Mn. The Fe  $L_{2,3}$  and Mn  $L_{2,3}$  edges are quite similar to those of the initial material. The Mn 2p electronic level displays one division of the  $L_2$  line (see arrows in Figure 10), which differs from initial hematite in which no fine structure could be resolved. We believe that this difference is due to a poorer signal-to-noise ratio of Mn spectra in the initial material, which contains less Mn than the newly formed hematite. Comparison with previously published data [Garvie *et al.*, 1994] strongly indicates prominent  $Mn^{3+}$  in hematite. All hematites (standard, or decomposition product of siderite) are characterized by similar Fe 2p spectra: the  $L_3$  line shows a strong density of multiplet at the lowest-energy side with a pre-peak at about 709 eV. The  $L_2$  line is split in two major features. Several experiments and theoretical calculations have demonstrated that these typical features are preserved for various local surroundings of  $Fe^{3+}$  ions. The effect of symmetry with different crystal field strength is mainly to shift the peak positions by a few tens of eV and to slightly change their intensities. For instance, the intensity of the  $L_3$  pre-peak of ferric iron is generally smaller for tetrahedral than for octahedral environments [Crocobette *et al.*, 1995; Van der Laan and Kirkman, 1992]. Keeping in mind that the structure of Mn-substituted hematite is not significantly different from the reference, we suggest that Mn-hematite does not contain detectable  $Fe^{2+}$  ions.

[18] In samples heated at 530°C, hematite coexists with Mn-ferrite with spinel structure and unit cell parameters close to those of magnetite (Figure 9b). The grain size of hematite does not significantly differ from samples heated at 480°C. Mn-ferrite appears as euhedral single crystals with grain sizes varying between 20 and 100 nm. The hematite EELS spectra show no difference with the lower temperature spectra and thus have not been reported in Figure 10. The Mn-ferrite phase was identified by diffraction patterns and EELS spectra (Figure 10). The EELS measurements at Fe 2p indicate a prevalent  $Fe^{3+}$  in this spinel; which is not expected for pure magnetite stoichiometry. The spectra at Fe  $L_{2,3}$  edges are very close to that of hematite (Figure 10). The

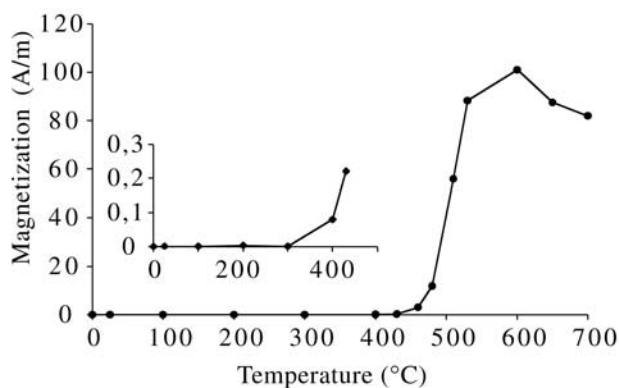


**Figure 7.** Acquisition of partial thermoremanent magnetization at incremental temperature steps.

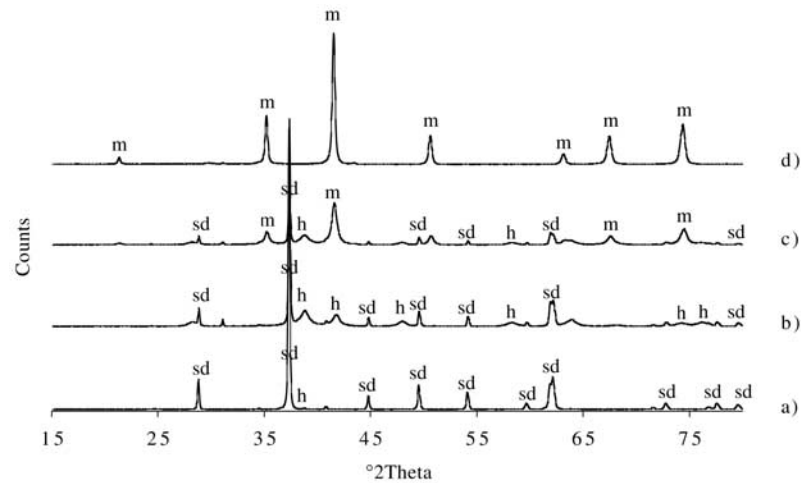


**Figure 8.** XRD spectra: (a) room temperature, (b) 480°C, (c) 530°C, and (d) 700°C. H, hematite; m, Mn-ferrite; sd, siderite.

pre-peak of  $L_3$  line located at around 709 eV is slightly weaker than in hematite spectrum, a likely signature of some tetra-coordinated  $\text{Fe}^{3+}$  ion in the spinel. In addition, no divalent iron contributions have been detected in this spinel. Indeed, a few percent of ferrous iron would have amplified

the pre-peak intensities, which is in contrast with the experimental observation. The EELS Mn  $L_{2,3}$  in Mn-ferrite exhibits a spatially inhomogeneous behavior. Three spectra collected for different crystals with a probe of 30nm in size, display different fine structures (Figure 10). They exhibit a

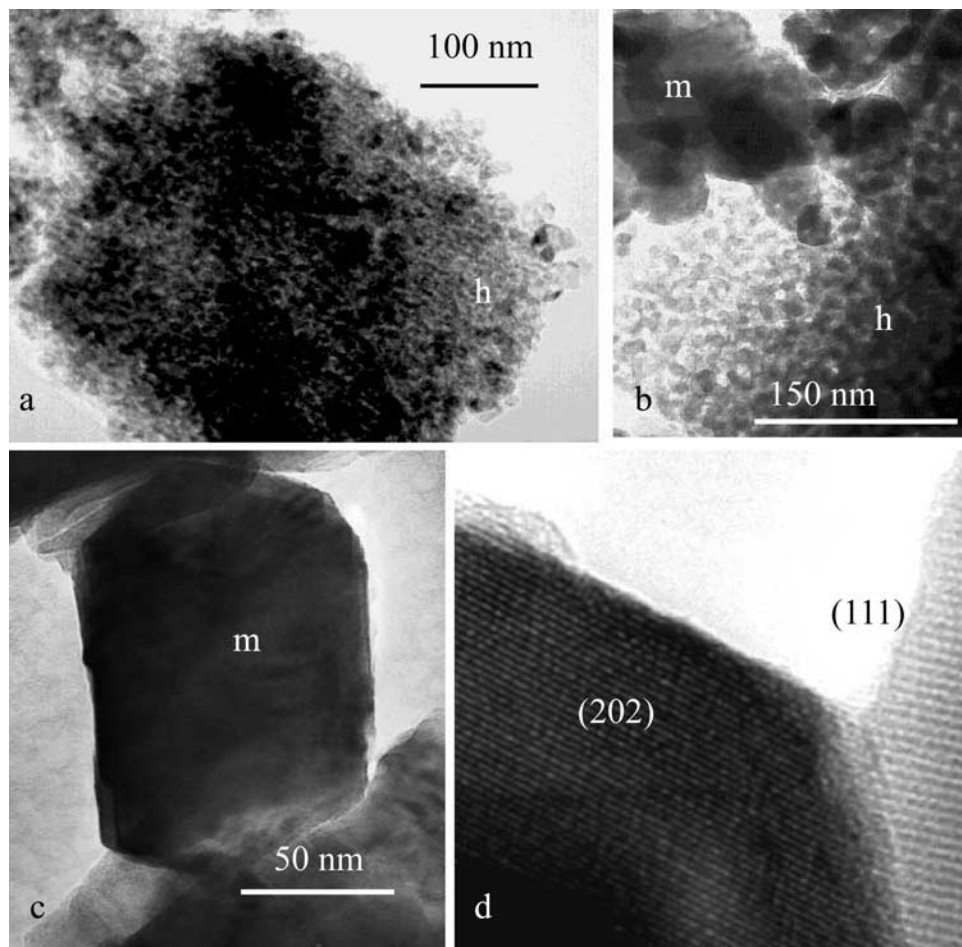


**Figure 9.** TEM images of siderite decomposition products: (a) 480°C, hematite (h) growing on a siderite crystal; (b) 530°C, Coexistence of coarse grained Mn-ferrite (m) and hematite (small grains); (c) 700°C, well-crystallized Mn-ferrite; (d) 700°C, HREM image of Mn-ferrite.

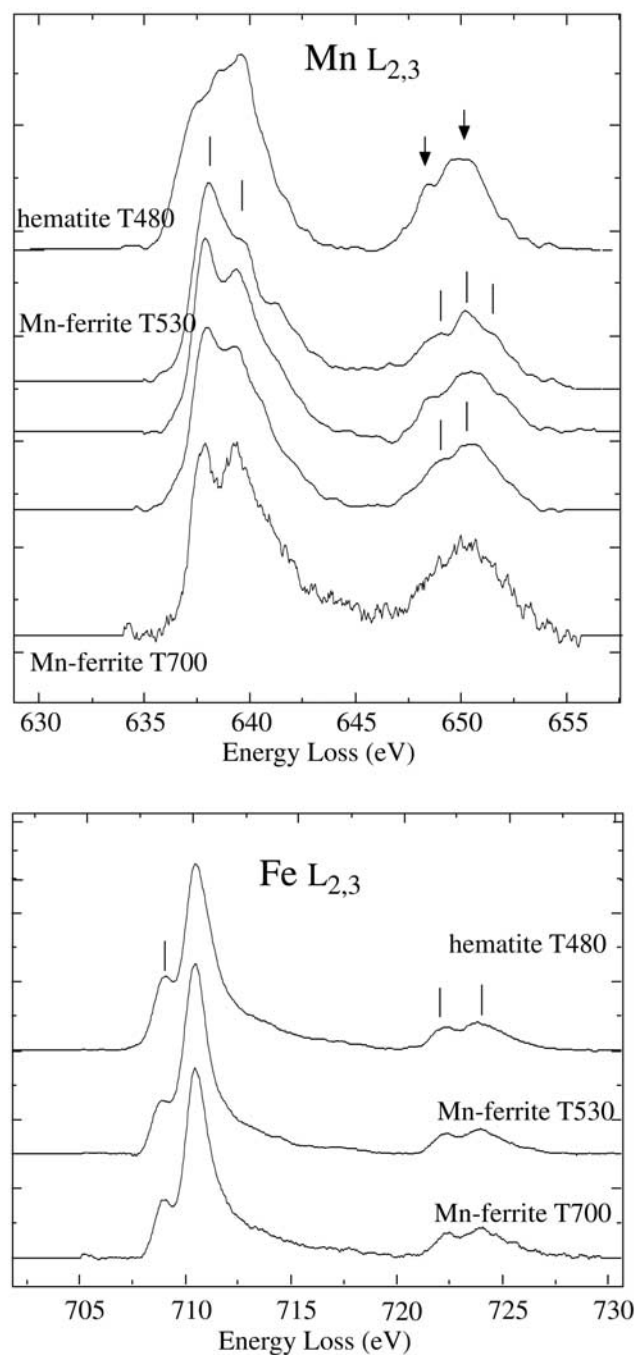


**Figure 10.** EELS spectra at Mn  $L_{2,3}$  and Fe  $L_{2,3}$  edges of siderite decomposition products.

strong splitting of the  $L_3$  line that could be considered as a mixed contribution of the sharp white line of  $Mn^{2+}$  (at 638 eV) and of the broad  $L_3$  line of  $Mn^{3+}$ . No quantitative method has been proposed to determine the valencies of Mn using Mn 2p EELS data. A crude estimate of mixed valencies could however be obtained using previously published Mn 2p XAS or EELS data of a known compound obtained with similar energy resolution. The spectrum showing the most intense  $Mn^{2+}$  contribution is in good agreement with the XAS experiment obtained by *Stichauer et al.* [2001] for a nanocrystalline film of Mn-ferrite and

may thus bear a largely prevailing  $Mn^{2+}$  ( $Mn^{2+}/Mn^{3+} > 3/2$  can be confidently assumed by comparison of the XAS data). The Mn 2p spectra are close to those of  $Mn_3O_4$  haussmanite and exhibit  $L_3$  line peaks of similar intensities [Garvie *et al.*, 1994]. We may infer that the most oxidized spinel at 530°C has a  $Mn^{2+}/Mn^{3+}$  ratio greater than 1/2.

[19] TEM images of samples heated at 700°C show Mn-ferrite only, which is consistent with XRD results. Grains of Mn-ferrite are often faceted-single-crystals (Figures 9c–9d) with sizes varying between 25 and 200 nm, most crystals being 90–100 nm in size. In the high-resolution micrograph in Figure 9d the lattice fringes of (202) and (111) are consistent with a spinel structure. The EELS spectra of Mn-ferrite unambiguously show the coexistence of mixed Mn valences in the spinel crystal that are close to those observed for haussmanite ( $Mn^{2+}/Mn^{3+} \approx 1/2$ ), but no heterogeneities have been detected in the samples. Here again, the spectra at Fe  $L_{2,3}$  edges are very similar to hematite (Figure 10), which suggests that most iron atoms in the Mn-ferrite phase are  $Fe^{3+}$  with certainly a contribution of fourfold coordinated ions.

## 5. Interpretation and Discussion

[20] The successive phases appearing upon oxidation of natural Mn and Mg-bearing siderite are reflected by drastic changes in the behavior of the thermomagnetic curves after heating at increasing temperature steps. They indicate two successive mineralogical transformations at 300°C–430°C and at 500°C. Both have been documented by XRD analyses and TEM observations.

[21] The first appearing ferromagnetic mineral was not observed microstructurally but was inferred only from magnetic measurements. This is possibly maghemite, which might have resulted from the transformation of minor phases in the starting material, and then rapidly transformed into hematite with increasing temperature. The XRD measurements did not detect the presence of maghemite but showed only hematite peaks at 480°C. This was confirmed also by the electron microscopic observations, which detected the presence of hematite growing up on siderite crystals with increasing temperature. The second ferromagnetic mineral was observed above 500°C and was identified as a spinel-structured Mn-ferrite [Housen *et al.*, 1996]. The EELS spectra reveal the coexistence of  $Mn^{2+}$  and  $Mn^{3+}$  in this spinel phase, which is thus a substituted maghemite or magnetite:  $(Mn^{2+}, Mg^{2+}, Fe^{3+})(Fe^{3+}, Mn^{3+})_2O_{3+\delta}$  stoichiometry. This is in agreement with the lattice parameters obtained by XRD, which are more similar to those of a maghemite standard than to magnetite. Similar to Fe substitution by titanium in titanomagnetites, the presence of Mn lowers the Curie temperature. In samples heated at 530°C, Mn-ferrite grains were observed with sizes varying between 25 and 100 nm approximately, which corresponds to either superparamagnetic or single-domain states. The presence of superparamagnetic grains was confirmed by the magnetic measurements of the remanence (Figure 6). Acquisition of thermoremanent magnetization revealed that the magnetic phase preserved the memory of the applied field above 430°C. At 480°C, nanometric single-domain ferrimagnetic grains were detected by all magnetic measurements. Hysteresis cycles indicate the presence of pseudo-single-domain-type grains, which satu-

rate at 0.2T, in accordance with magnetite values. At 700°C neither hematite, nor maghemite, nor siderite were detected in the XRD analyses and TEM observations. The Mn-ferrite spinel phase is indeed the final product.

[22] A previous study was carried out by Pan *et al.* [2000] to document the behavior of pure siderite in air. Diffraction analyses and susceptibility cycles were performed on relatively pure crystalline siderite (with minor quartz and calcite). A first low field thermomagnetic experiment was conducted up to 510°C and then two other cycles up to 700°C. A major difference with our results is that the thermomagnetic cooling curves were found below the heating curves for pure siderite, except during the first cycle at 510°C. After successive heating cycles, siderite was decomposed into a ferrimagnetic phase and subsequently converted into another phase of weaker susceptibility. In our case, there was production of a strong magnetic phase with a decrease of the Curie point with increasing annealing temperature. In contrast, Pan *et al.* [2000] did not detect hematite but magnetite at 490°C; at 580°C they observed that siderite, hematite and maghemite were coexisting whereas at 690°C maghemite and hematite were revealed by diffraction, but siderite and magnetite were then absent. Their analyses thus indicate that siderite decomposed first into magnetite, then into maghemite, ultimately into hematite. In this case, the final oxidation product of siderite was hematite. Thus this sequence is almost opposite to the present observations in which hematite (and not magnetite) grew up first while Mn-ferrite appeared at about 530°C and persisted as final product (and not hematite). This difference emphasizes the important role of Mn, which is often present in natural siderites, as a stabilizer of spinel-structured phases carrying stable magnetization.

## 6. Conclusion

[23] As opposed to pure siderite, we have shown that Mn-bearing siderite is characterized by different oxidation products during heating in air. These differences are caused by the presence of Mn in the siderite crystal lattice. Similar to titanium in magnetite, Mn stabilizes the structure of the spinel phase. This explains the presence of stable remanence signals that were acquired after transformation and also why Mn-ferrite is the final product of oxidation of Mn-bearing siderite. The existence of stable remanence linked to such transformation may have profound implications in paleomagnetism of buried or heated material. The processes involved in such changes are evidently important in order to constrain further the magnetic properties of carbonated rocks with temperature. Transformation of siderite at room temperature might also create magnetite and thus have important implications for magnetic studies of siderite in sediments [Ellwood *et al.*, 1988]. Additional studies are needed to investigate whether similar Mn-ferrite can be formed from Mn-siderite, without heating.

[24] **Acknowledgments.** The authors are pleased to acknowledge Dominique Gasquet from ENSG in Nancy for having provided us with siderite and Maxime Le Goff and Hélène Bouquerel for their assistance in the magnetic experiments. We would like to thank Claude Michel from the CRISMAT ISMRA laboratory of Caen University for the ATG measurements and Michel Fialin for the electron probe microanalyses. We also acknowledge Josh Feinberg, Brooks Ellwood, and Rudy Wenk for their comments, which improved this manuscript.

## References

- Barber, D. J., and E. R. D. Scott, Origin of supposedly biogenic magnetite in the Martian meteorite Allan Hills 84001, *Proc. Natl. Acad. Sci. USA*, *99*, 6556–6561, 2002.
- Brearley, A. J., Magnetite in ALH84001: Product of decomposition of ferrous carbonate (abstract), *Lunar Planet Sci.*, *XXIX*, abstract 1451, 1998.
- Cressey, G., C. M. B. Henderson, and G. Van der Laan, Use of L-edge X-ray Absorption Spectroscopy to characterize multiple valence states of 3d transition metals: A new probe for mineralogical and geochemical research, *Phys. Chem. Minerals*, *20*, 111–119, 1993.
- Crocobette, J. P., M. Pollack, F. Jolet, N. Thromat, and M. Gautier-Soyer, X-ray absorption spectroscopy at Fe  $L_{2,3}$  threshold in iron oxides, *Phys. Rev. B*, *52*, 3143–3150, 1995.
- Ellwood, B. B., W. Balsam, B. Burkart, G. J. Long, and M. L. Buhl, Anomalous magnetic properties in rocks containing the mineral siderite: Paleomagnetic implications, *J. Geophys. Res.*, *91*, 12,779–12,786, 1986.
- Ellwood, B. B., T. H. Chrzanowski, F. Hrouda, G. J. Long, and M. L. Buhl, Siderite formation in anoxic deep-sea sediments: A synergetic bacterially controlled process with important implications in paleomagnetism, *Geology*, *16*, 980–982, 1988.
- Friedmann, E. I., J. Wierzchos, C. Ascaso, and M. Winklhofer, Chains of magnetite crystals in the meteorite ALH84001: Evidence of biological origin, *Proc. Natl. Acad. Sci. USA*, *98*, 2176–2181, 2001.
- Garvie, L. A. J., and P. R. Buseck, Ratio of ferrous to ferric iron from nanometer-size areas in minerals, *Nature*, *396*, 667–669, 1998.
- Garvie, L. A. J., A. J. Craven, and R. Brydson, Use of electron-energy loss near edge fine structure in the study of minerals, *Am. Mineral.*, *79*, 411–425, 1994.
- Gloter, A., A. Douri, M. Tencé, and C. Colliex, Improving Energy resolution of EELS spectra: An alternative to the monochromator solution, *Ultramicroscopy*, in press, 2003.
- Golden, D. C., D. W. Ming, C. S. Schwandt Jr., H. V. Lauer, R. A. Socki, R. V. Morris, G. E. Lofgren, and G. A. McKay, A simple inorganic process for formation of carbonates, magnetite, and sulfides in Martian meteorite ALH84001, *Am. Mineral.*, *86*, 370–375, 2001.
- Housen, B. A., S. K. Banerjee, and B. M. Moskowitz, Low-temperature magnetic properties of siderite and magnetite in marine sediments, *Geophys. Res. Lett.*, *23*, 20,2843–20,2846, 1996.
- Kozioł, A. M., Magnetite and carbonate textures in ALH84001: Experimental insights, *Lunar Planet. Sci.*, *XXXII*, abstract 1425, 2001.
- McKay, D. S., Jr., E. K. Gibson, K. L. Thomas-Keptra, H. Vali, C. S. Romanek, S. J. Clemett, D. F. Chilliier, C. R. Maechling, and R. N. Zare, Search for past life on Mars: Possible relic biogenic activity in Martian meteorite ALH84001, *Science*, *273*, 924–930, 1996.
- Pan, Y., R. Zhu, S. K. Banerjee, J. Gill, and Q. Williams, Rock magnetic properties related to thermal treatment of siderite: Behaviour and interpretation, *J. Geophys. Res.*, *105*, 783–794, 2000.
- Peng, G., J. Van Elp, H. Jang, L. Que, W. H. Armstrong, and S. P. Cramer, L-edge X-ray Absorption and X-ray magnetic circular dichroism of oxygen-bridged dinuclear iron complexes, *J. Am. Chem. Soc.*, *117*, 2515–2519, 1995.
- Seguin, M., Instability of FeCO<sub>3</sub> in air, *Am. J. Sci.*, *264*, 562–568, 1966.
- Stichauer, L., et al., X-ray absorption spectroscopy and magnetic circular dichroism of the Mn-ferrite nanocrystalline thin films, *J. Appl. Phys.*, *90*, 2511–2516, 2001.
- Thomas-Keptra, K. L., D. A. Bazylinsky, J. L. Kirschvink, S. J. Clemett, D. S. McKay, S. J. Wentworth, H. Vali Jr., E. K. Gibson, and C. S. Romanek, Elongated prismatic magnetite crystals in ALH84001 carbonate globules: Potential Martian magnetofossils, *Geochim. Cosmochim. Acta*, *45*, 4049–4081, 2000.
- Thomas-Keptra, K. L., S. J. Clemett, D. A. Bazylinsky, J. L. Kirschvink, D. S. McKay, S. J. Wentworth, H. Vali Jr., E. K. Gibson, M. F. McKay, and C. S. Romanek, Truncated hexa-octahedral magnetite crystals in ALH84001: Presumptive biosignatures, *Proc. Natl. Acad. Sci.*, *98*, 2164–2169, 2001.
- Van Aken, P. A., B. Liebscher, and V. J. Styras, Quantitative determination of iron oxidation states in minerals using Fe  $L_{2,3}$ -edge electron energy-loss near-edge structure spectroscopy, *Phys. Chem. Min.*, *25*, 323–327, 1998.
- Van der Laan, G., and I. W. Kirkman, The 2p absorption spectra of 3d transition metal compounds in tetrahedral and octahedral symmetry, *J. Phys. Condens. Matter*, *4*, 4189–4204, 1992.

A. Gloter, Laboratoire de Physique des Solides, Université Paris Sud, bat 510, UMR 8502, F-91405 Orsay, France. (gloter@lps.u-psud.fr)

F. Guyot, Laboratoire de Minéralogie et de Cristallographie de Paris, Institut de Physique du Globe de Paris, 4 place Jussieu, F-75252 Paris cedex 05, Paris, France. (guyot@lmpc.jussieu.fr)

A. Isambert and J.-P. Valet, Institut de Physique du Globe de Paris, Laboratoire de Paléomagnétisme, 4 Place Jussieu, F-75252 Paris cedex 05, France. (isambert@ippg.jussieu.fr; valet@ippg.jussieu.fr)